JOURNAL OF MATERIALS SCIENCE 28 (1993) 6040 6049

Microstructure and properties of aluminium tungsten oxide ceramics synthesized by a high power cw CO_2 laser*

XINGJIAO LI, FANG ZHENG
Department of Solid State Electronics, Huazhong University of Science and Technology, Wuhan, People's Republic of China

QIGUANG ZHENG, JIARONG LI, ZAIGUANG LI
National Laboratory of Laser Technology, HUST, Wuhan, People's Republic of China

SHAOPING LI
Materials Research Laboratory, The Pennsylvania State University, University Park, PA 16802, USA

Laser powder sintering has been used as a new technique to synthesize electronic ceramics consisting of the Al_2O_3–WO_3 system. Examination of the products by scanning electron microscopy and energy dispersive X-ray spectroscopy showed that cell structure and lateral intergrowth crystals formed in the specimens. The depth distribution of the elemental composition of the sample changed in an amplitude modulated manner. A comparison of the properties of the samples synthesized by laser and/or conventional sintering methods showed that the laser technique can produce new substances with some unique properties, such as a linear decrease in the resistivity of Al_2O_3–50 mol% WO_3 specimens with increasing temperature over the range 10°–150°C. X-ray photographic powder analysis indicated that the conducting phase in the specimen is non-equilibrium product: Al_xWO_3 tungsten bronze. The experiments also showed that the conductivity of samples was related to their composition and microstructure.

1. Introduction

Lasers as a directed energy source can be applied to electronic materials for the processing and modification of the surface layers of semiconductors. In the process of laser irradiation, the materials are melted. The quench rates of the melt are so fast that new structures, metastable phases and essentially perfect epitaxial single crystal materials with good electrical properties can be fabricated. Another striking indication of the use of laser irradiation as a tool for surface processing is that dopants could be incorporated on lattice sites at concentrations far exceeding their solid solubilities. The possibility of using this sophisticated surface heating technique should be considered for such processes as the laser annealing of ion-implanted semiconductors and the alloying of metal layers for contact formation during the fabrication of semiconductor devices [1].

The laser sintering method is a new technique initiated by Japanese scientists in 1984 [2] and used later by others [3, 4] for synthesizing high toughness, high hardness and high melting point ceramics from ceramic oxide powders. According to these researchers, this method has some particular advantages that are not possessed by conventional sintering methods [2–4]. Artificial materials with new phases can be fabricated because of the different absorption coefficients of various ceramic powders, and the larger heating and quenching rates. Linking characterization of electrical materials to laser sintering allows prediction of the feasibility of the synthesis of electronic ceramics.

Aluminum tungsten oxide has been found to have extensive applications in a number of fields, one of them being catalysis. It is noteworthy to point out the instructive parallelism between the homogeneous and heterogeneous catalyst versions [5, 6]. It has also been considered as a tunable laser material after its single crystal was doped with chromium [7, 8]. The material inherently has features that could be further exploited if it is subjected to a manufacturing process that somehow produces useful properties. Laser synthesizing, because it has some unique processing characteristics, like fast heat and quench rates, was used to produce new and exciting thermosensitive ceramics with semiconducting properties and particular microstructure from this Al_2O_3–WO_3 system.

2. Experimental Procedure

2.1. Preparation of a pelletized mixture of Al_2O_3 and WO_3

The oxides used in this work were analytical grade

* Supported by the National Natural Science Foundation of China and the National Education Ministry of China.

0022–2461

Al_2O_3 and WO_3 powders. After being wet ball-milled, the powders were dried, added to polyvinyl alcohol and then pressed into cylinders 15 mm in diameter and 3 mm in thickness. The ceramic powder compacts were calcined at 300 °C for 1 h and then kept at 100 °C prior to use.

2.2. Synthesis of Al_2O_3–WO_3 system ceramics using a laser

The laser used in these experiments was CO_2, 10.6 μm, continuous wave laser with a maximum power output of 2 kW. The experimental laser irradiation system is schematically illustrated in Fig. 1. The calorimeter was used to check the beam power before every run. The power density on the sample was controlled by changing the laser power and the position of the sample relative to the focal point of the final focusing mirror. The laser was operated in miltimode. The spot size of the laser beam on the sample was generally adjusted to the same size as the diameter of the sample, 15 mm.

During the sintering procedure, the laser beam was directed onto the sample with a continuous power output of 0–2 kW. At the maximum power sintering was allowed to continue for several seconds, depending on the sample, and then the laser was switched off.

2.3. Synthesis of Al_2O_3–50 mol% WO_3 ceramics by conventional sintering in a furnace

Due to the evaporation of WO_3 the ceramics synthesized in a furnace were made by the following in-house process. It is applicable for producing ceramics using compositions that have a low vapour pressure. The Al_2O_3–WO_3 powder pellets were sealed inside Al_2O_3 powder, forming an "outer compact" using a larger die. The ceramics were produced by heating in air at 1150 °C, cooling naturally in the furnace, and then removing the Al_2O_3 powder.

2.4. Measurement of the electrical conductivity

For electrical measurements both surfaces of the samples were ground flat and smooth. Silver paint was applied on both surfaces to enhance electrical contact and then dried in an oven at 120 °C. Resistance of the samples was measured at room temperature using a two probe method. For measuring the resistivity of the samples as a function of temperature, a temperature chamber with a range of 10–200 °C and an accuracy of ± 1% was used.

I–V characteristics of some selected samples were examined using an oscilloscope (model Vp-5220) and the circuit shown in Fig. 2.

2.5. Characterization of the products

The crystalline phases in the products were identified by powder X-ray diffraction (XRD) and photographic powder techniques. A scanning electron microscope (SEM) equipped with energy dispersive spectroscopy (EDS) was employed for morphologic examination and determination of depth profiles of the elemental composition in samples. Heat tests ranging up to 1400 °C were conducted in differential thermal analysis-thermogravimetry (DTA-TG) equipment.

3. Microstructure of laser synthesized ceramics and the depth profiles of their elemental composition

3.1. Microstructure

3.1.1. Cellular structure

The common microstructural features of the laser-synthesized specimens, 30–70 mol% WO_3, are shown in Fig. 3. It gives an optical photograph and a series of surface and cross-sectional scanning electron micrographs (SEMs) of specimens subjected to various treatments. Fig. 3a shows the following specimens: the three round ones on the left were synthesized by laser, the two round ones on the upper right were synthesized by conventional sintering, and the three square ones were laser-synthesized ceramics shaped into thermistors. Fig. 3b–d shows the surface and cross-sectional SEM micrographs of a 50 mol% WO_3 specimen that exhibits the formation of cellular structure in the near-surface 1–2 mm region of the sample. It reveals that during laser irradiation, the upper half of the compact had melted and recrystallized to form fine polycrystals, while the lower half of the sample retained the characteristics of the furnace sintering. It also contains a few holes resulting from WO_3 gasification, i.e. part of the compact had not been melted. In

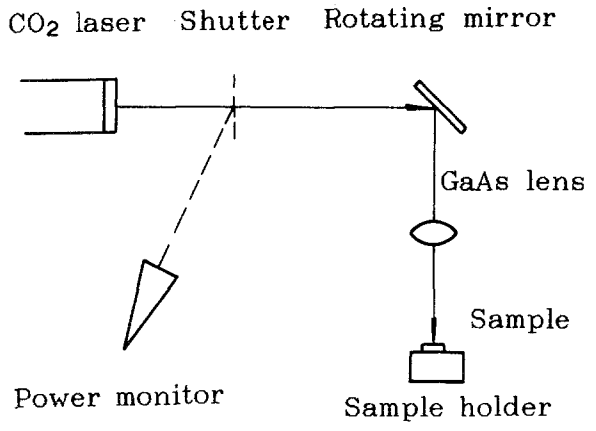

Figure 1 Schematic of a laser irradiation system.

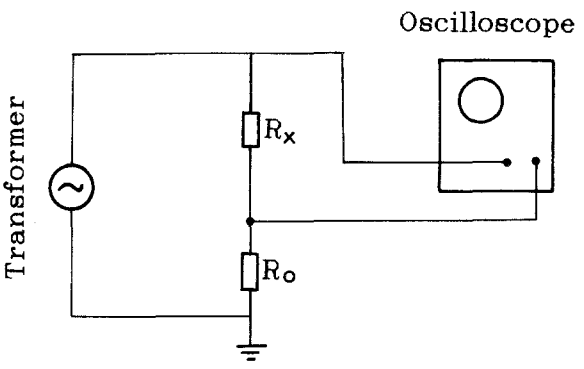

Figure 2 Circuit for I–V characteristic of specimens

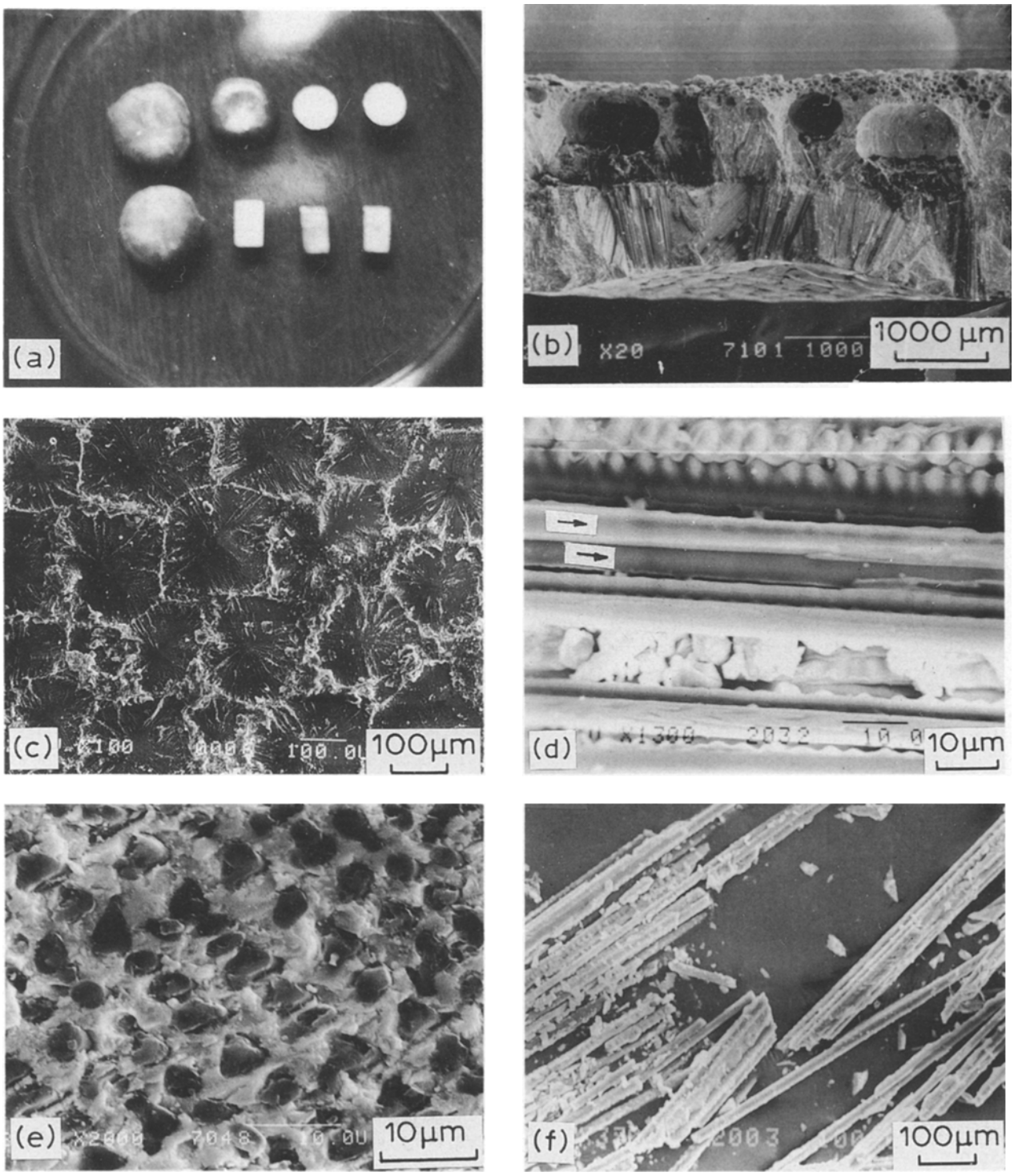

Figure 3 Photograph of specimens (a) and scanning electron micrographs of an Al_2O_3–50 mol% WO_3 specimens: (b, d) cross-section; (c) tetragonal network of grooves and pyramids on the surface; (e) two dimensional array of the pockets of Al_2O_3 single crystals; (f) Al_2O_3 single crystal cellular structure.

the interior of each cell in Fig. 3b are the columns of Al_2O_3 single crystals that grew from the unmelted part of the sample up to the surface. Fig. 3f shows the crystals and Fig. 4 the oscillation photographs of Al_2O_3 crystals about the c_0 axis, $c_0 = 1.293$ nm. Surrounding each column of single crystals is a thin cell wall containing massive concentrations of aluminum tungstates and channels of precipitated phases, which form the boundaries of the cells. Fig. 3e shows the black spots of the cross-sections of these columns and reveals a two-dimensional periodic array of these column crystals in the recrystallized materials. The cross-links between the parallel grooves result in the tetragonal network grooves and tetragonal pyramids ultimately formed on the surface. These are shown in Fig. 3b–f and are apparently formed as a result of the segregation behaviour when zones of constitutional supercooling occurred in the resolidifying melt. The characteristic spacing in the resulting cell structure is given very roughly by D/v [9], where D is the impurity

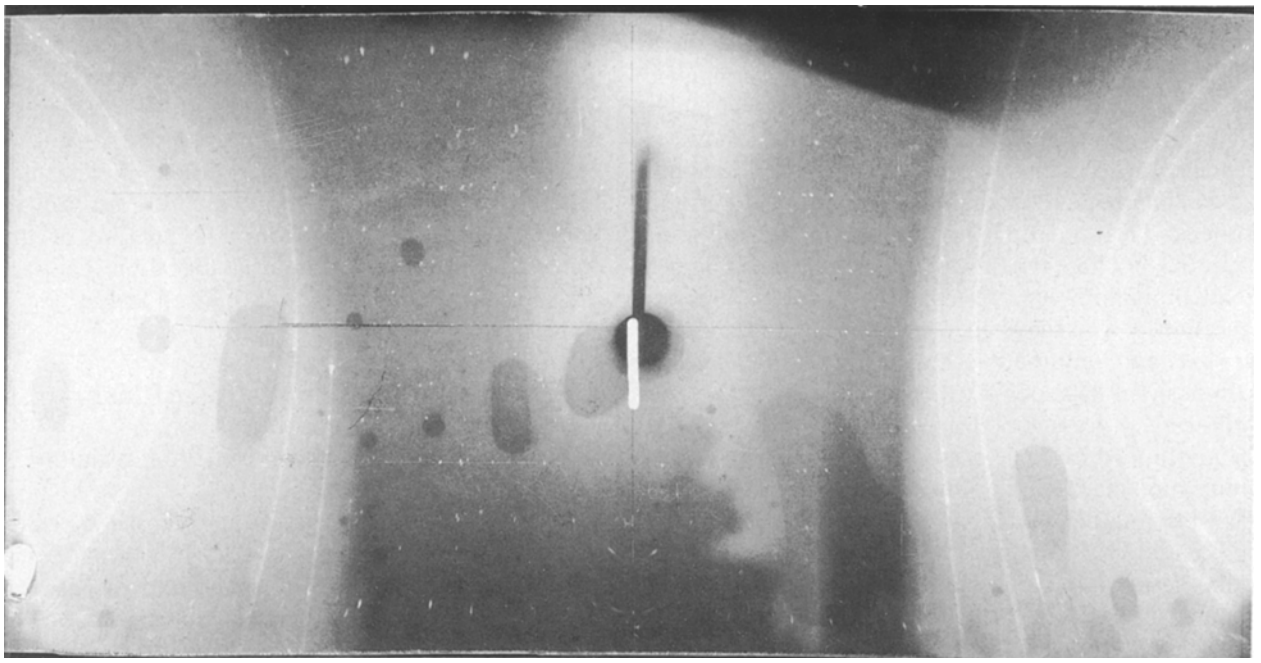

Figure 4 Oscillation photographs of Al_2O_3 crystals about the c_0 axis, $c_0 = 12.93$.

diffusion coefficient and v is the crystal growth velocity. Taking D to be typically 10^{-5} cm s^{-1}, and letting v be ~ 0.1 cm s^{-1}, $D/v = 1$ μm, which, for the approximations involved, compares favourably with the observed interchannel dimensions of ~ 5 μm.

It is worthwhile mentioning that a similar situation occurs for the cell structure in Q-switched laser annealing of ion-implanted layers of semiconductors, such as Fe-implanted silicon layers [10]. In that case, however, the velocity of the recrystallization interface is often 1–5 m s^{-1}, much greater than the conventional growth rates 10^{-5}–10^{-2} cm s^{-1} [11, 12]. The conditions of Q-switched laser annealing and laser sintering under which this cell structure occurs have provided new experimental results for testing the theory of crystal growth.

3.1.2. Lateral intergrowth crystals

In particular, for one Al_2O_3–80 mol % WO_3 specimen, analysis of SEM photographs (Fig. 5) shows that cell structure arising from lateral segregation of the rejected solute caused by an interfacial instability that develops during regrowth is not formed. Instead of cell structure, fine crystallites emerged, having some grains with black and colourless laterally intergrown crystals (Fig. 5a). Fig. 5b shows that this black phase was surrounded by other phases. If the conducting phase was separated by non-conducting material, that may explain why ceramics with a composition of 80 mol % WO_3 have a high resistivity, as shown in the next section.

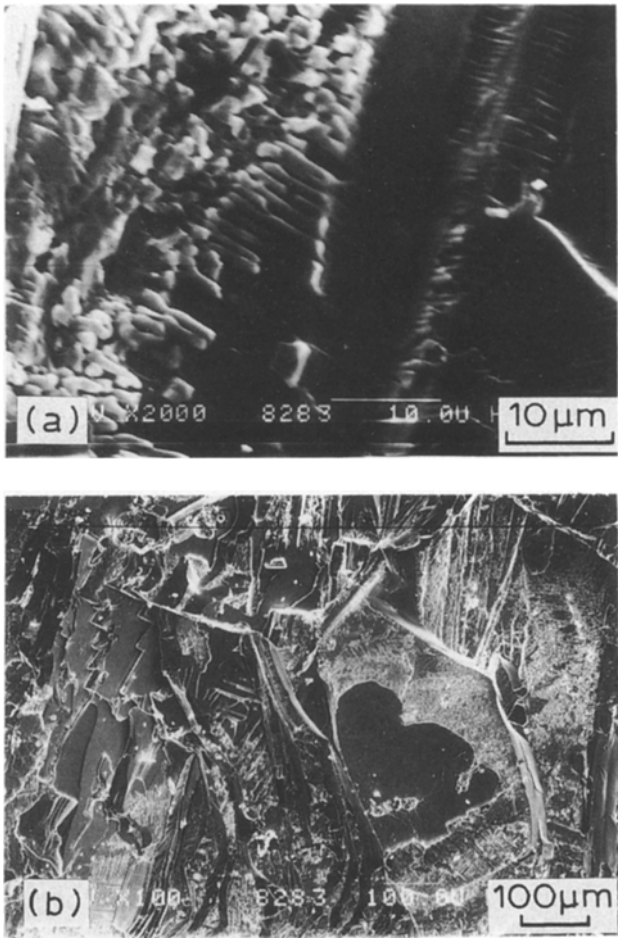

Figure 5 Cross-sectional scanning electron micrographs of a 80 mol % WO_3: (a) lateral intergrowth crystals; (b) a crystal surrounded by other phases, similar to a peritectic system.

3.2. The depth profiles of tungsten and aluminum contents

Another important consideration is the depth profiles of the relative concentrations of tungsten and aluminium. To answer this question, energy dispersive X-ray (EDX) spectroscopy was performed. The results are shown in Fig. 6. The oxygen concentrations indicated are calculated results. Fig. 6a shows aluminium, tungsten and oxygen depth distribution at the single

crystal lying in the upper left-hand corner of Fig. 3d (indicated by the arrow). The contents of the three elements changed in an amplitude modulated manner as depth decreased, and aluminium content was much higher than tungsten. In addition, it also shows a tendency to a higher tungsten content the lower the aluminium content at shallow depth, e.g. close to the surface. This situation also occurs in the cell wall (Fig. 6b), but here the tungsten content is much higher than aluminium. As a result of these observations we questioned why tungsten was found in Al_2O_3 single crystals and why the depth distribution of elemental composition had such a variation. It is likely that the following process was responsible for the impurity being trapped in single crystals occurring at the resolidification interface. The rapid movement of the interface ensured that some tungsten atoms were en-gulfed in the quickly forming solid Al_2O_3 before they could diffuse away into the liquid. By their non-equilibrium nature, the interfacial distribution coefficients K' are considerably greater than the corresponding equilibrium values and depend on the high growth velocities of the crystals. Furthermore, if, in crystal growth

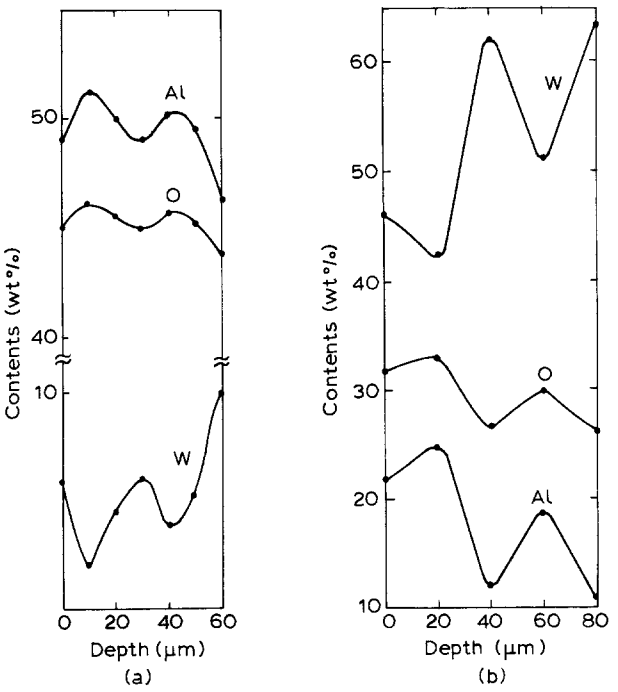

Figure 6 Depth profiles of Al, W and O contents in: (a) a single crystal; (b) the thin cell wall.

$K' < 1$ (where $K' = C_s/C_L$; C_s and C_L are concentrations of solute in solution in the solid and liquid phases at the interface) as solidification proceeds, then solute will accumulate in the liquid at the interface so that a higher solute content appears near the surface. The amplitude modulated distribution of elemental composition explains the fact that both the growth velocity and K' are not constant, because of the complex temperature during resolidification. This fact is also proven by the waves of cell wall in Fig. 3d.

4. The electrical properties of laser synthesized ceramics

4.1. Linear negative temperature coefficient effect

To investigate the material's properties, as a first step XRD analysis was undertaken to identify the phases in the obtained ceramics. The results and the general properties of the ceramics are shown in Table I. The results indicate that $Al_2(WO_4)_3$ was formed. This seems to be different from the Al_2O_3–WO_3 equilibrium phase diagram, in which Waring showed that Al_2O_3 reacts with WO_3 to produce an intermediary compound $2Al_2O_3{\cdot}5WO_3$ [13]. Accordingly, Okutomi *et al.* misinterpreted $Al_2(WO_4)_3$ as a substance not existing in the Al_2O_3–WO_3 equilibrium phase diagram and as being produced under a non-equilibrium process [14, 15]. Craig and Stephenson determined the structure of the compound reported by Waring as $2Al_2O_3{\cdot}5WO_3$ in the Al_2O_3–WO_3 equilibrium phase diagram early in 1968 and showed that the formula of this oxide should be $Al_2(WO_4)_3$ [16]. Therefore, the results in Table I support the results of Craig and Stephenson and are in fact consistent with the Al_2O_3–WO_3 equilibrium phase diagram.

Fig. 7 shows the X-ray diffraction patterns of Al_2O_3–50 mol % WO_3 samples synthesized respectively, by (a) use of a laser and (b) the conventional sintering methods. Comparing the two patterns, it is difficult to find any difference between them except for the intensities of the peaks. However, the laser synthesized ceramics are indeed different from these produced in a furnace . In comparing the 50 mol % WO_3 samples, first, the colours of the ceramics are different: the former is black while the latter is white. Both Al_2O_3 and $Al_2(WO_4)_3$ are white powders, and the furnace ceramic can therefore be considered normal.

TABLE I Properties of the synthesized materials

Composition (mol %)	Sintering method	Colours	Phases	Resistivity (Ω cm) at 298 K
Al_2O_3–$10WO_3$	Laser	Black	Al_2O_3, $Al_2(WO_4)_3$	$> 10^9$
Al_2O_3–$20WO_3$	Laser	Black	Al_2O_3, $Al_2(WO_4)_3$	$10^8 \sim 10^9$
Al_2O_3–$30WO_3$	Laser	Black	Al_2O_3, $Al_2(WO_4)_3$	$\sim 10^5$
Al_2O_3–$40WO_3$	Laser	Black	Al_2O_3, $Al_2(WO_4)_3$	$\sim 10^4$
Al_2O_3–$50WO_3$	Laser	Black	Al_2O_3, $Al_2(WO_4)_3$	$\sim 10^1$
Al_2O_3–$60WO_3$	Laser	Black	Al_2O_3, $Al_2(WO_4)_3$	$\sim 10^2$
Al_2O_3–$70WO_3$	Laser	Blackish green	Al_2O_3, $Al_2(WO_4)_3$	$\sim 10^1$
Al_2O_3–$80WO_3$	Laser	Green	$Al_2(WO_4)_3$, WO_3	$\sim 10^7$
Al_2O_3–$90WO_3$	Laser	Greenish-yellow	$Al_2(WO_4)_3$, WO_3	$\sim 10^3$
Al_2O_3–$50WO_3$	Conventional	White	Al_2O_3, $Al_2(WO_4)_3$	$> 10^9$

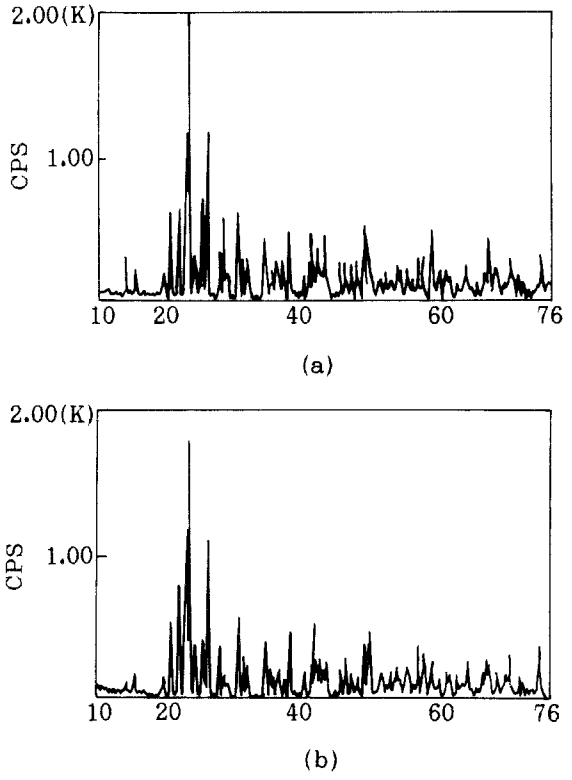

Figure 7 X-ray diffraction spectra from specimens produced by: (a) a laser sintering method; (b) a conventional sintering method.

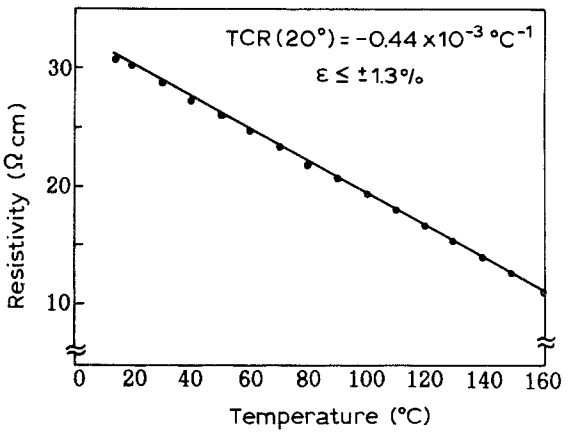

Figure 8 R–T characteristics of a laser synthesized Al_2O_3–50 mol% WO_3 sample.

Second, the electrical properties of laser and furnace ceramics are also distinguishable. The former is a semiconductor with a resistivity of about 30 Ω cm at 298 K and has a negative temperature coefficient (NTC) effect. From 10 °C to 150 °C its resistance decreases linearly with increasing temperature (Fig. 8), and its I–V curve is symmetrical about the origin (Fig. 9). The latter is just an insulator. Third, they have different thermal behavior. DTA-TG measurements, showed laser ceramics having an endothermic peak at 539 °C that was accompanied by a loss of weight of 2.4% above 512 °C. The sample melted when a temperature of 1225 °C was reached. The furnace ceramic melted at 1225 °C, but without any loss of weight. In another experiment the laser-synthesized specimen was heated above 600 °C, especially at 900 °C for 1 h. The colour of the sample changed from black to faint

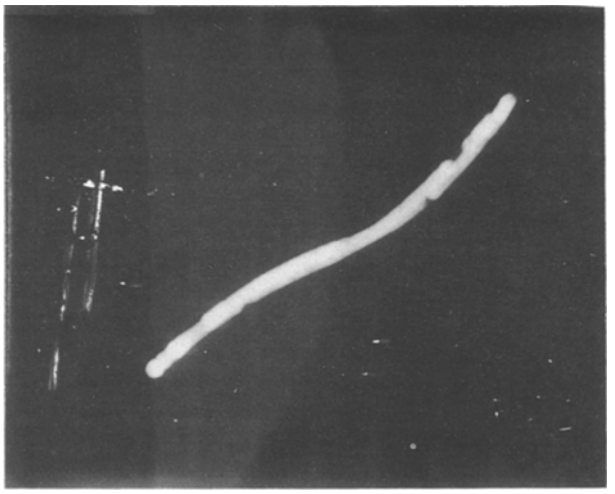

Figure 9 I–V characteristics of a laser synthesized Al_2O_3–50 mol% WO_3 specimen.

yellow and its resistivity rapidly increased and tended to be non-conducting. All these differences stimulated us to investigate these materials in detail.

4.2. X-ray photographic powder analysis

For exact phase identification of the ceramics, the X-ray photographic powder technique was used. Diffraction patterns were recorded with a Guinier camera (model FR 550) for 15 h using silicon oxide-filtered $CuK_{\alpha 1}$ X-rays from a high power generator (mode RU-200B).

The powder data from a Guinier photograph (Fig. 10a), which had been corrected by a silicon inner standard, are listed in Table II and shown in total 140 lines. Confirming our original assertion, there was no doubt from Fig. 7 that the spectrum showed the main crystalline phase of the ceramics to be $Al_2(WO_4)_3$. The interplaner (d) spacings and relative intensities of the diffraction lines of the substance needed to be calculated to classify all the lines in the experimental powder pattern of the ceramics due to the limited data in the ASTM card. The calculation for all $h\,k\,l$ reflections was based on [17]. In the calculation procedure the absorption factor, a constant for all lines in the pattern, has been omitted and the temperature factor was not considered. A least-squares program was used to obtain the lattice constants. For laser synthesized $Al_2(WO_4)_3$, the lattice constants were $a_0 = 9.158(8)$, $b_0 = 12.625(4)$, $c_0 = 9.077(3)$. There were four formula units of $Al_2(WO_4)_3$ per unit cell. The volume of the unit cell at 298 K was 1.0496 nm^3.

The calculation was carried out until all d-values and the relative intensities of the possible 310 kinds of Bragg reflections corresponding to $h^2 + k^2 + l^2 > 59$ were obtained. Comparing the observed d-values with the calculated ones and considering $I \neq 0$, 123 lines were attributed to $Al_2(WO_4)_3$. The theoretical results corresponding to these lines were listed in Table II. Comparison of the residual lines with powder diffraction data cards of possible substances and a careful analysis of all diffraction lines concluded that the ceramics are composed of $Al_2(WO_4)_3$, Al_xWO_3, WO_3 (existing above 770 °C) and Al_2O_3.

TABLE II X-ray powder data for a laser synthesized Al_2O_3–50 mol % WO_3 specimen

d_A(calc)	d_A(obs)	hkl	I/I_0[a]	Phases[b]
6.3127	6.307	020	9(20)	a
5.7419	5.741	111	19(34)	a
4.5387	4.537	002	10(24)	a
4.5106	4.5162	121	5(12)	a
4.3050	4.3058	210	43(64)	a
4.0667	4.0715	102	51(67)	a
3.8897	3.8902	211	41(77)	a
		001		c
3.8709	3.8751	112	44(71)	a
3.8181	3.8241	031	100(100)	a
		202		b
	3.7713	040		b
3.7068	3.7077	220	15(38)	a
		001		c
3.6851	3.6850	022	9(27)	a
3.5241	3.5268	131	23(53)	a
	3.4887	132	(31)	b
		012		d
3.4317	3.4358	221	58(84)	a
3.2236	3.2257	202	18(44)	a
3.1563	3.1574	040	6(19)	a
		101		c
3.1234	3.1238	212	4(14)	a
		321		b
3.0987	3.1014	230	6(22)	a
2.9424	2.9434	013	16(48)	a
2.9325	2.9340	231	11(42)	a
2.9244	2.9256	132	6(27)	a
2.8710	2.8714	222	12(35)	a
2.8205	2.8211	311	10(29)	a
2.8014	2.8013	113	1(5)	a
		322		b
	2.6938	242	(3)	b
		111		c
2.6305	2.6315	321	5(19)	a
		200		c
2.6150	2.6166	123	16(44)	a
2.5988	2.5989	240	7(24)	a
		411		b
	2.5579	420	(44)	b
		104		d
2.5332	2.5334	302	8(24)	a
2.4985	2.4979	241	4(20)	a
2.4837	2.4839	312	4(19)	a
2.4755	2.4766	213	5(19)	a
		124		b
2.4327	2.4326	051	4(13)	a
2.3844	2.3852	331	3(33)	a
2.3728	2.3743	133	20(53)	a
		110		d
2.3510	2.3516	322	1(8)	a
2.3440	2.3439	223	3(10)	a
2.2897	2.2894	400	2(7)	a
2.2693	2.2689	004	2(10)	a
2.2553	2.2542	242	5(22)	a
2.2529		410	1	a
2.2112	2.2113	250	9(30)	a
2.2027	2.2030	104	2(9)	a
		440		b
2.1866	2.1882	411	20(49)	a
		201		c
		044		b
2.1699	2.1696	114	1(19)	a
2.1649	2.1651	233	3(11)	a
2.1525	2.1523	420	3(16)	a
2.1484	2.1484	251	4(22)	a
2.1355	2.1362	024	4(14)	a
2.1247	2.1242	143	3(11)	a
2.1186	2.1195	313	5(18)	a
2.1042	2.1040	060	6(22)	a

TABLE II. continued

d_A(calc)	d_A(obs)	hkl	I/I_0[a]	Phases[b]
2.0944	2.0914	421	1(50)	a
		211		c
2.0797	2.0823	124	1(2)	a
		113		d
2.0344	2.0342	323	1(8)	a
2.0075	2.0081	214	10(32)	a
1.9878	1.9868	252	3(10)	a
1.9756	1.9758	342	9(26)	a
1.9637	1.9632	431	1(4)	a
		204		d
1.9448	1.9461	422	6(22)	a
		002		c
1.9387	1.9383	053	2(14)	a
1.9120	1.9114	260	2(17)	a
		404		b
1.9090	1.9087	062	3(16)	a
1.8967	1.8971	153	2(6)	a
		080		b
1.8710	1.8707	261	6(36)	a
1.8534	1.8538	440	14(38)	a
		220		c
1.8425	1.8422	044	8(24)	a
		102		c
1.8309	1.8311	234	3(10)	a
		371		b
1.8070	1.8077	413	1(4)	a
1.8026	1.8014	314	2(7)	a
1.7970	1.7967	015	4(15)	a
1.7884	1.7878	352	3(14)	a
1.7764	1.7752	343	2(5)	a
1.7690	1.7688	071	2(5)	a
1.7621	1.7624	262	1(10)	a
1.7634		115	2	a
1.7499	1.7499	324	3(1)	a
	1.7437	024	(27)	d
1.7369	1.7369	171	2(5)	a
		112		c
1.7271	1.7266	521	4(13)	a
1.7158	1.7157	442	7(24)	a
		602		b
1.7094	1.7086	244	3(11)	a
		206		b
1.7018	1.7016	361	2(8)	a
1.6979	1.6978	163	5(16)	a
		282		b
	1.6839	211	(14)	c
1.6750	1.6751	433	6(19)	a
1.6728		215	1	a
1.6673	1.6673	451	1(10)	a
		190		b
		091		b
1.6599	1.6606	154	2(5)	a
		310		c
1.6502	1.6507	271	3(12)	a
		425		b
		560		b
1.6403	1.6404	522	1(5)	a
		065		b
1.6304	1.6305	225	9(30)	a
1.6118	1.6129	404	10(33)	a
		236		b
	1.6057	301	(46)	c
		116		d
1.5988	1.5991	414	1(6)	a
1.5837	1.5833	254	6(19)	a
1.5775	1.5781	344	4(23)	a
		202		c
	1.5669	642	(8)	b
1.5664	1.5666	235	2(4)	a
1.5617	1.5611	424	1(3)	a
1.5551	1.5549	513	4(12)	a

TABLE II. continued

d_A(calc)	d_A(obs)	hkl	I/I_0[a]	Phases[b]
1.5493	1.5492	073	3(16)	a
1.5486		315	1	a
		211		d
1.5306	1.5315	371	3(9)	a
		311		c
1.5276	1.5274	173	1(5)	a
1.5215	1.5215	164	2(15)	a
1.5154	1.5156	610	3(14)	a
		122		d
1.5035	1.5036	363	1(3)	a
		212		c
1.4958	1.4970	542	3(9)	a
1.4883	1.4882	245	2(4)	a
1.4823	1.4820	116	1(4)	a
1.4796	1.4786	453	2(4)	a
1.4643	1.4646	621	4(17)	a
1.4553	1.4549	155	1(6)	a
1.4526	1.4529	126	2(6)	a
1.4468	1.4463	602	1(4)	a
1.4355	1.4353	444	2(11)	a
1.4350		630		a
1.4273	1.4275	216	1(7)	a
1.4174	1.4175	631	3(17)	a
1.4094	1.4088	552	4(27)	a
		124		d
1.4000	1.3998	543	1(31)	a
	1.3769	321	(29)	c
		030		d
1.3643	1.3640	046	4(13)	a
	1.3575	222	(4)	c
1.3556	1.3549	306	3(9)	a
1.3550		613	1	a
1.3477	1.3481	435	8(27)	a
1.3478		316	1	a
1.3322	1.3316	623	1(2)	a
		125		d
	1.3258		(12)	c
1.3152	1.3161	642	1(13)	a
	1.3060		(8)	c
1.2855	1.2844	711	1(6)	a
	1.2790	208	(25)	d
	1.2661		(2)	c
1.2622	1.2613	406	2(10)	a
1.2572	1.2571	702	2(12)	a
1.2484	1.2478	712	1(7)	a
1.2393	1.2405	624	1(10)	a
1.2351	1.2364	731	1(6)	a
		1010		d
1.2304	1.2317	722	1(4)	a
	1.2156		(2)	c
	1.1850	220	(7)	d
	1.1611	306	(4)	d

[a] The data in parentheses are observed values.
[b] Phases: (a) $Al_2(WO_4)_3$; (b) Al_xWO_3; (c) WO_3; (d) Al_2O_3.

From Table II, it is seen that the calculated intensities were generally smaller than the observed ones, but they coincided with the results shown in Fig. 7 and the data of the ASTM card. There are two reasons for this: one is the omission of the temperature factor during calculation, and the other is the peak overlap of various phases and the complex factors affecting the relative integrated intensity during the experiments. For the observed results listed in Table II the highest peak has not reached its expected value, therefore the relative intensities of all weaker peaks become larger.

4.3 The formation of the Al_xWO_3 phase under non-equilibrium

How Al_xWO_3 was formed during laser irradiation required an answer. From the Al_2O_3–WO_3 equilibrium phase diagram it would seem impossible that Al_2O_3 reacts with WO_3 to produce Al_xWO_3. To form this compound there must have been metallic tungsten or reduced tungsten oxide present [17, 18]. This implies that WO_3 had been partly reduced during laser irradiation, and for this two mechanisms were possible. (1) WO_3 was reduced by carbon, the component of the graphite sample holder: between 650 and 850 °C carbon reduces WO_3 to medium oxides, between 900 and 1050 °C to WO_2, and at 1200 °C to metallic tungsten. (2) WO_3 is either dissociated losing oxygen under a lower oxygen partial pressure at high temperature or by a multiphoton absorption effect, and then turned into the reduced tungsten oxides which contain a series of crystallographic sheared planes resulting from the removal of the oxygen defects.

$$WO_3 \xrightarrow{h\nu} WO_{3-x} + \tfrac{x}{2}O_2$$

The first case is unimportant, because during laser irradiation a little Al_2O_3 powder was added underneath the compacts. For the specimens with a WO_3 content of less than 60 mol % the bottom never melted during the experiment. When we used a corundum sample holder instead of the original graphite one, the same black ceramics with the Al_xWO_3 phase were obtained. Thus, it is more reasonable to suppose that the reduced tungsten oxides were formed by the second mechanism.

To examine this mechanism further, Al_2O_3–50 mol % WO_3 material was synthesized in a furnace with a N_2 or Ar atmosphere under non-equilibrium

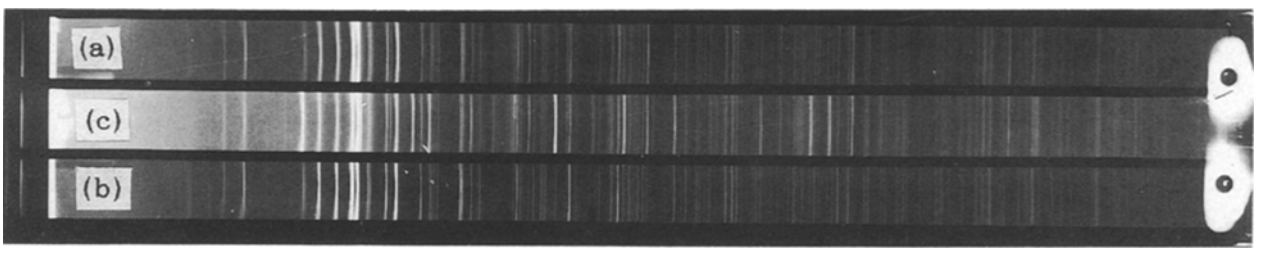

Figure 10 Guinier patterns of the Al_2O_3–50 mol % WO_3 specimens produced by: (a) laser sintering; (b) conventional sintering; (c) production in N_2 or Ar gas.

conditions. Black ceramics with resistivity of 40.1Ω cm at 298 K and a negative temperature coefficient effect were obtained. Fig. 10 shows the Guinier patterns of Al_2O_3–50 mol% WO_3 samples synthesized, respectively, by (a) laser, (b) conventional sintering and (c) in a reducing atmosphere. Comparing them, one concludes that all of them have the same main crystalline phase $Al_2(WO_4)_3$, but (b) lacks the diffraction lines with *d*-values equal to 3.82, 3.78 and the range 2.5–2.9 corresponding to a Al_xWO_3 phase.

It must be noted that it is under non-equilibrium condition that Al_xWO_3 was formed in laser-synthesized Al_2O_3–50 mol % WO_3 samples. Apparently, during laser irradiation the temperature of compacts was far above 500 °C at which Al_xWO_3 oxygenates. However, due to the high heating and cooling rates of the specimen, Al_xWO_3 had been trapped in the samples before the slower oxygenation could take place. Therefore, the non-equilibrium process was a decisive factor for producing aluminium tungsten bronze in laser-synthesized specimens.

4.4. Discussion of the material conducting phase

A review of what constitutes a tungsten bronze is given in [20–22]. Al_xWO_3 tungsten bronze in the laser-synthesized specimens is a perovskite related bronze. The lattice constants of this orthorhombic substance are $a_0 = 10.871(6)$, $b_0 = 15.152(8)$, $c_0 = 10.778(6)$, and the volume of the unit cell equals 1.775604 nm^3. According to [18, 19], it is a semiconductor. From the properties of the bronze it is easy to understand the experimental results of Section 4.1. Due to the formation of Al_xWO_3, the laser-synthesized samples were black and lustrous. The conductivity of Al_xWO_3 results in the ceramics being semiconductors and having a negative temperature coefficient effect. Although WO_3 is a semiconductor by itself, its resistivity at 298 K was about 10^5 Ω cm, much larger than the 30 Ω cm of the laser-synthesized specimen. In Al_2O_3–50 mol% WO_3 samples, WO_3 was not present in excess to react and form $Al_2(WO_4)_3$, thus Al_xWO_3 played an important role in the conductivity of the ceramics. It explains the observed DTA-TG results that WO_3 volatilizes above 500 °C and bronzes can be oxygenated to form fully oxidized compounds and WO_3, according to the following

$$\tfrac{4}{3x}Al_xWO_3 + O_2 \xrightarrow{>540°C} \tfrac{2}{3}Al_2(WO_4)_3 + (\tfrac{4}{3x} - 2)WO_3$$

The electrical measurements showed the materials with higher aluminium content to have larger resistivities. For laser-synthesized ceramics it can be deduced from the depth distribution of the composition that the depth values of the resistivity also changed in an amplitude-modulated fashion. Thus, a possible mechanism for the linear variation of ceramic resistivity versus temperature is the compensation between resistivities, similar to a string of thermistors having different temperature coefficients. However, to probe this problem more electrical measurements must be done, and this is the subject of our work in the near future.

6. Summary

In the present paper, the following tenets are offered.

1. Laser sintering is a feasible method for synthesizing electronic ceramics. With it NTC semiconductor materials have been obtained consisting of an Al_2O_3–WO_3 system.
2. Laser synthesized ceramics have some unique properties that are not produced by conventional sintering methods. One of these is the valuable property of a linear resistivity decrease with increasing temperature over the range 10–150 °C for the Al_2O_3–50 mol % WO_3 thermistors.
3. The non-equilibrium product, aluminium tungsten bronze Al_xWO_3, plays an important role in the electrical conductivity of the material.
4. The cellular structure emerges in the laser synthesized 30–70 mol% WO_3 specimens. For 80 mol% WO_3 samples excellent crystallites were formed, in which, for some grains, black and transparent crystals laterally intergrew, and for others one phase irregularly interdispersed into another phase.
5. The depth profiles of the elemental compositions change in an amplitude modulated manner and the conductivity of the laser-synthesized specimens is closely related to their compositions and microstructure.

Acknowledgements

The author would like to thank Mr Jianse Liu for assisting during the experiments and Mr Wuda Shu for carrying out the furnace sintering work.

References

1. J. M. POATE, in "Laser Annealing of Semiconductors", Edited by J. M. Poate and James W. Mayer (Academic Press, New York, 1982) p. 1.
2. M.OKUTOMI, M. KASAMATSU, K. TSUKAMOTO, S. SHIRATORI and F. UCHIYAMA, *Appl. Phys. Lett.* **44** (1984) 1132.
3. XINJIAO LI, T. C. BAI, F. LIANG, F. ZHENG, H. HE, Q. G. ZHENG, J. R. LI and Z. G. LI, in "Thin Films and Beam–Solid Interactions, Vol. 4, Proceedings of the C-MRS International '90", Edited by Liji Huang (Elsevier, The Netherlands, 1991) p. 579.
4. JIRONG LI, Q. C. ZHENG, X. TAO, X. Q. TAO, Z. LI, X. J. LI, F. LIANG and F. ZHENG, *Zhong Gou Ji Guang* **18** (1991) 770.
5. W. GRUENERT, E. S. SHPIRO, R. FELDHAUS, K. ANDERS, G. V. ANTOSHIN and Kh. M. MINACHEV, *J. Catal.* **107** (1987) 522.
6. Yu. S. KHODAKOV, K. ANDERS, A. N. SUBBOTIN, V. S. NAKHSHUNOV, R. FELDHAUS and S. NOWAK, *Izv. Akad. Nauk SSSR, Ser. Khim.* **8** (1981) 1724.
7. K. PETERMANN and P. MITZSCHERLICH, *IEEE J. Quantum Electron.* **QE-23**(7) (1987) 1122.
8. K.PETERMANN and G. HUBER, *J. Lumin.* **31–32**(1) (1984) 71.
9. B. R. PAMPLIN, in "Crystal Growth" (Pergamon Press, Sydney, 1975) p. 40.
10. A. G. CULLIS, H. C. WEBBER, J. M. POATE and N. G. CHEW, *J. Microsc.* **118** (1980) 41.

11. W. BARDSLEY, J. S. BONLTON and D. T. J. HURLE *Solid-State Electron.* **5** (1962) 395.
12. W. W. MULLINS and R. F. SEKERKA, *J. Appl. Phys.* **35** (1964) 444.
13. J. WARING, *J. Amer. Ceram. Soc.* **48**(9) (1965) 493.
14. M. OKUTOMI, *Tool Eng.* **31**(7) (1987) 53.
15. M. OKUTOMI, *KiNouZaiRyou* **7**(8) (1987) 11.
16. D. C. CRAIG and N. C. STEPHENSON, *Acta Crystallogr.* **B24** (1968) 1250.
17. H. P. KLUG and L. E. ALEXANDER, in "X-ray Diffraction Procedures for Polycrystalline and Amorphous Materials" (Wiley, London, 1973) p. 120.
18. M. POUCHARD, F. BERDOULAY and D. VANDEVEN, *C.R. Acad. Sci. Paris* Sec. C. **266**(14) (1968) 1066.
19. D. VANDEVEN, J. GALY, M. POUCHARD and P. HAGENMULLER, *Mater. Res. Bull.* **2** (1967) 809.
20. T. EKSTROM and R. J. D. TILLEY, *Chemica Scripta* **16** (1980) 1.
21. P. HAGENMULLER, in "Comprehensive Inorganic Chemistry", Vol. 4. Edited by J. C. Bailer, H. J. Emeleus, Sir. R. Nyholm and A. F. Trotman–Dickenson (Pergamon Press, Oxford, 1973) p. 541.
22. P. G. DICKENS and P. J. WISEMAN, in "M. T. P. International Review of Sci. Inorganic Chemistry, Series 2, Vol. 10. Edited by L. E. J. Roberts (Butterworths, London, 1974) p. 211.

Received 17 June 1992
and accepted 4 January 1993